Direct Study on the Unimolecular Decomposition of Methoxy Radicals: The Role of the Tunneling Effect

Tatsuo Oguchi, Akira Miyoshi,* Mitsuo Koshi, and Hiroyuki Matsui

Department of Chemical System Engineering, The University of Tokyo, 7-3-1 Hongo, Bunkyo-ku, Tokyo 113-8656

(Received August 19, 1999)

The unimolecular decomposition of methoxy radicals, $CH_3O+M \rightarrow CH_2O+H+M$ (1a), has been directly studied by laser photolysis–laser-induced fluorescence method in the temperature range 610—740 K. Nearly linear pressure dependence of the first-order decay rate was observed in the investigated pressure range (100—450 Torr), and the second-order rate constants were derived for He and N_2 buffer gases as: $k^0(\mathrm{He}) = 2.8\times10^{-9}\exp(-84.3\ \mathrm{kJ\,mol^{-1}}/RT)$ $\mathrm{cm^3\,molecule^{-1}\,s^{-1}}$ and $k^0(N_2) = 4.3\times10^{-9}\exp(-84.1\ \mathrm{kJ\,mol^{-1}}/RT)$ $\mathrm{cm^3\,molecule^{-1}\,s^{-1}}$, respectively. An RRKM calculation with a semiclassical one-dimensional tunneling treatment showed that the tunneling effect is essentially important in the present experimental conditions. The calculation indicates a non-linear pressure dependence of the rate constant even in the classical low-pressure limiting conditions, which is consistent with the experimental observations. The RRKM model (with threshold energy = 101.7 $\mathrm{kJ\,mol^{-1}}$) derived by the best fit to the experimental results is in good agreement with the theoretical investigations and the microcanonical rate constants measured by the stimulated emission pumping method.

The methoxy radical is one of the important reaction intermediates in combustion and atmospheric photooxidation of hydrocarbons. In the conditions of combustion, the radical is mainly removed by its thermal decomposition:

$$CH_3O+M \rightarrow CH_2O+H+M$$
$$\Delta H^\circ_{0K} = (83.1\pm5.3)\ \mathrm{kJ\,mol^{-1}} \quad (1a)$$

at the temperatures above ca. 500 K, in competition with the dominant fate at around room temperature:

$$CH_3O+O_2 \rightarrow CH_2O+HO_2. \quad (2)$$

Since the laser-induced fluorescence (LIF) spectrum of the methoxy radical was found by Inoue et al.,[1] several kinetic studies on the bimolecular reactions with O_2,[2—4] NO_2,[5—7] and NO,[8—12] have been reported in the last two decades. Only one direct measurement on the thermal decomposition rate[13] has been reported. However, recently, Choudhury et al.[14] reported one to two orders of magnitude higher rate constant for the thermal decomposition than the value from direct measurements[13] or the earlier recommended value.[15] Although they explained their large rate constants and the small activation energy in terms of the tunneling effect, the large discrepancy between their and earlier measurements should be resolved by further direct investigations. It should be noted that the direct investigations on the thermal decomposition of larger alkoxy radicals, i-C_3H_7O[16] and t-C_4H_9O,[17] have been reported recently.

Several ab initio calculations at relatively high levels (MRCI, G2) have been reported[18—20] including the unimolecular isomerization of methoxy radical;

$$CH_3O+M \rightarrow CH_2OH+M.$$
$$\Delta H^\circ_{0K} = (-39.1\pm8.5)\ \mathrm{kJ\,mol^{-1}} \quad (1b)$$

Since the barrier height for the reaction (1b) has been predicted to be about 28 $\mathrm{kJ\,mol^{-1}}$ higher than that for (1a),[19] the dominant unimolecular process will be the C–H bond fission (1a).

Temps and co-workers[21,22] have investigated the unimolecular dynamics of methoxy radical by the stimulated emission pumping (SEP) method. They reported the state resolved microcanonical rate constants above and below the classical reaction threshold. Their real-time measurement on the unimolecular decay rate in 10^6—10^8 $\mathrm{s^{-1}}$ range, performed well below the classical threshold, indicates the importance of the tunneling in this reaction.

In the present work, the unimolecular decomposition process of the methoxy radicals has been investigated by laser photolysis–laser-induced fluorescence method in the temperature range of 610—740 K and pressure range of 100—450 Torr (1 Torr $\approx$ 133.322 Pa) with He or N_2 buffer gas. The results were analyzed by an RRKM calculation with one-dimensional tunneling treatment, and were compared with the theoretical investigations and the previous experimental measurements on the microcanonical rate constants. The effect of tunneling on the unimolecular processes in the low-pressure limit regime is discussed. Also the possible contribution of the isomerization process (1b) is discussed based on the RRKM calculation with theoretical threshold energy.

Experimental

Experiments were carried out by laser flash photolysis–laser induced fluorescence (LIF) technique in a slow flow reactor, similar to

that used in the previous experiments.[23] A schematic of the apparatus is shown in Fig. 1. The tubular quartz reactor was confined in an electric furnace which can be heated up to 800 K. The temperature was regulated within ±2 K.

The methoxy radicals were generated by the pulsed ArF excimer laser (Lambda Physik LEXTRA50) photolysis of methanol at 193 nm:

$$CH_3OH + h\nu \rightarrow CH_3O + H \quad (3a)$$

$$\rightarrow CH_2OH + H, \quad (3b)$$

for which the channel (3a) is known to be the main channel ($\phi_{3a} : \phi_{3b} = 0.86$: ca. 0[24] or 0.54 : 0.08[25]). The methoxy radicals were detected by exciting the ν_3: (4′–0″) band of $\tilde{A}$–$\tilde{X}$ transition around 293 nm. The probe light was generated by a XeCl excimer laser (Lambda Physik LEXTRA200)–pumped dye laser (Lambda Physik LPD3002, Rhodamine 6G) with a frequency doubling. The fluorescence was detected by a photomultiplier (Hamamatsu R374) through color glass filters (HOYA UV22, UV28, and U340). The signal from the photomultiplier was amplified and averaged using a boxcar integrator (Stanford Research SR250), and was stored in a personal computer. The concentration vs. time profiles were recorded by scanning the delay time between the photolysis and probe laser pulses.

Gas flows were regulated using mass flow controllers and gases were premixed before entering the reactor. The typical linear flow velocity was ca. 27 cm s^{-1}, at which the gas refresh rate in the cell was ca. 1 Hz. The experimental data were obtained at higher photolysis rate, 7 Hz, after confirming that no difference was found between the results at 1 Hz and 7 Hz. The total pressures in the reactor were measured using a capacitance manometer (MKS Baratron 122A). Carrier gases, He (Nippon Sanso, >99.9999%) and N_2 (Nippon Sanso, >99.9995%), were used as delivered. Methanol (Wako, Spectra grade) was degassed, diluted by He, and stored in a glass reservoir. The concentration of methanol in the reactor was kept around 2.0×10^{14} molecules cm^{-3} and the fluence of the photolysis laser was around 10 mJ cm^{-2}. The typical concentration of methoxy radicals was about 6×10^{11} molecules cm^{-3}.

Under such low initial concentration of methoxy radicals, the effect of side reactions such as CH_3O+H is negligible. For example, at $[CH_3O]_0 = [H]_0 \approx 6\times10^{11}$ molecules cm^{-3}, the CH_3O+H reaction ($k = 3.0\times10^{-11}$ cm^3 molecule^{-1} s^{-1})[26] contributes the decay rate of CH_3O by only ca. 10 s^{-1}, while the measurements were done at unimolecular decay rates of 460—12000 s^{-1}. The reaction of H atoms, produced by the photolysis (3) or by the decomposition of CH_3O (1a), with methanol

$$H + CH_3OH \rightarrow CH_2OH + H_2 \quad (4a)$$

$$\rightarrow CH_3O + H_2 \quad (4b)$$

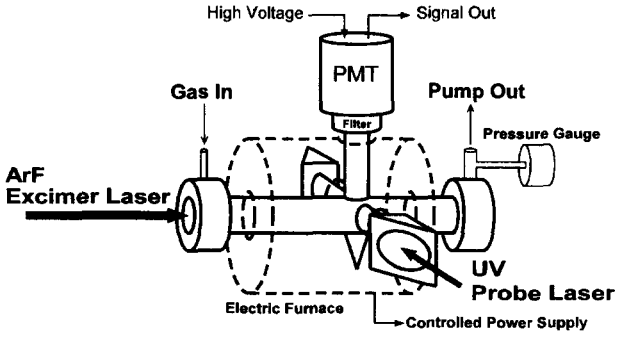

Fig. 1. Schematic of the experimental apparatus.

may regenerate CH_3O via channel (4b). However, from the rate constant (ca. 2×10^{-12} cm^3 molecule^{-1} s^{-1} at 700 K) and the branching fraction ($f_{4b} \approx 2\%$ at 700 K),[27] the effect of this reaction was estimated to be negligible. Further, these were verified experimentally: That is, no change of the decay rate was observed when the initial concentration of methanol changed in the range of 1.0—4.0×10^{14} molecules cm^{-3}. Although the photolytic generation may produce the vibrationally hot methoxy radicals, the effect of the vibrational excitation was concluded to be negligible since 1) hot bands around 295 nm, ν_3:(6′–1″), ν_3:(5′–1″), and ν_3:(4′–1″), were not observed in the fluorescence excitation spectrum recorded at relatively low pressure (120 Torr, He) and at short delay time (70 μs) between photolysis and probe laser shots, and 2) the decay of methoxy radical well fits the single exponential function.

The experiments were performed at pressures >100 Torr in order to avoid the effect of diffusion loss of the methoxy radicals. The measured decay rates of the methoxy radicals at room temperature, where the diffusion loss is the dominant decay process, were plotted against the total pressure in Fig. 2. The contribution of the diffusion loss (<90 s^{-1}) was negligible under the pressures above 100 Torr.

Results

Typical decay profiles of the methoxy radicals at elevated temperature are shown in Fig. 3. The first-order decay rates of methoxy radicals depend almost linearly on the total pressures. Figure 4 summarizes the decay rates measured as a function of the temperature and the pressure with He buffer gas. The solid lines in Fig. 4 indicate the results of linear regression, and the second-order rate constants were derived from the slopes at each temperature.

It should be noted that the linear regression *without* constraint to the origin (broken lines in Fig. 4) indicates positive intersects at $P = 0$. This seems to be reasonable from the nonlinear pressure dependence predicted by the RRKM calculation with tunneling treatment, which will be discussed in detail in the next section. The second-order rate constants derived here were rather phenomenological, but necessary for the comparison with previous studies. Figure 5 compares the Arrhenius plot of the second-order rate constants derived in the present study with those from the previous studies. The Arrhenius expressions for the present results are:

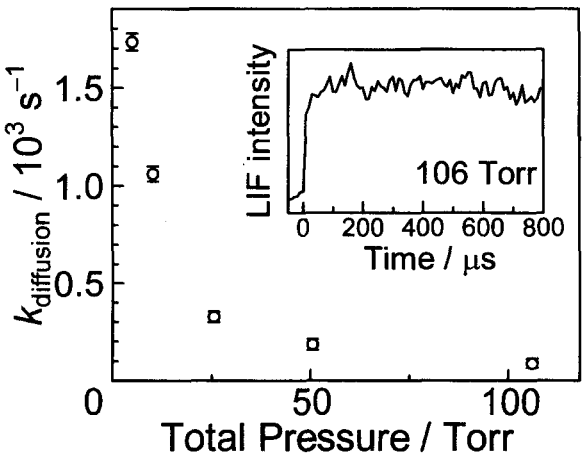

Fig. 2. Observed diffusion loss rates ($k_{diffusion}$) of methoxy radicals at room temperature (He buffer).

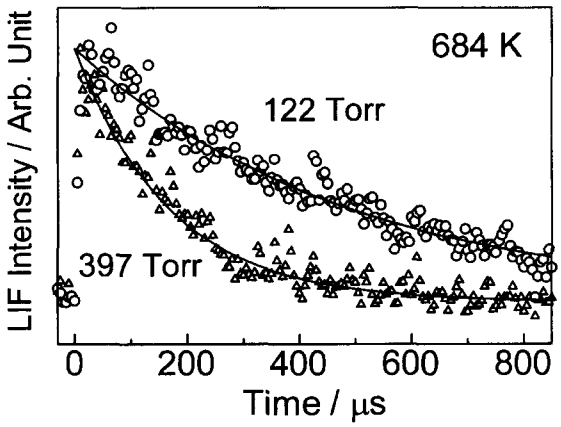

Fig. 3. Typical decay profiles of the methoxy radicals at elevated temperature (He buffer).

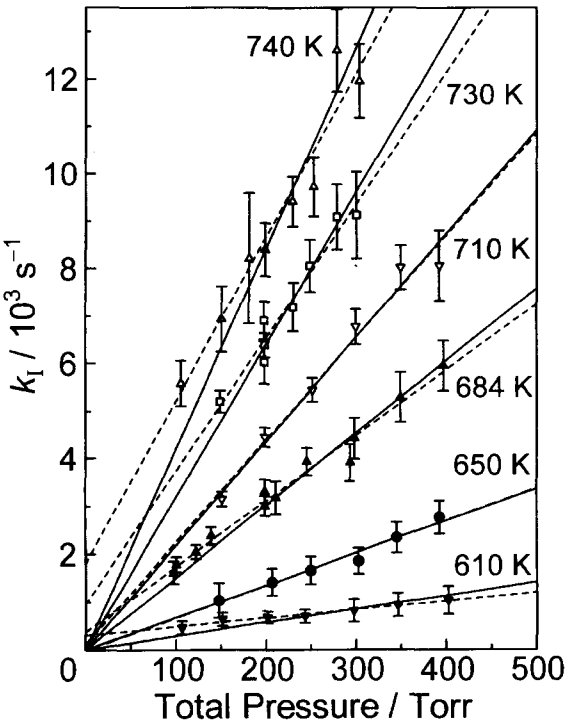

Fig. 4. Observed first-order decay rate (k_I) of methoxy radicals (He buffer). Solid lines (—): results of the linear regression with constraint to the origin ($k = 0$ at $P = 0$). Broken lines (- - -): results of the linear regression without constraint. Error bars denote the two standard deviations derived from the least-squares analysis of decay profiles.

$$k^0(\mathrm{He}) = (2.8 \pm 0.3) \times 10^{-9} \exp((-84.3 \pm 2.5)\mathrm{kJ\,mol^{-1}}/RT)\ \mathrm{cm^3 molecule^{-1}\,s^{-1}},$$

$$k^0(\mathrm{N_2}) = (4.3 \pm 1.0) \times 10^{-9} \exp((-84.1 \pm 7.5)\mathrm{kJ\,mol^{-1}}/RT)\ \mathrm{cm^3\,molecule^{-1}\,s^{-1}}.$$

The present rate constants are larger than the evaluation by Tsang and Hampson[15] but still smaller than those reported by Choudhury et al.[14] Closer agreement was found with the previous direct measurements by Wantuck et al.,[13] but they are about two times smaller than the present study. The reason for this discrepancy with the similar direct measurement is not clear, but it should be noted that the measurements by Wantuck et al.[13] were done in lower pressure region (25—175 Torr), the photolysis region in the reactor is very small (3×3 mm), and thus the diffusion loss of the methoxy radical might significantly enlarge the decay rate at lower pressure and might result in the smaller second-order rate constants. The activation energy reported by Choudhury et al.[14] (56.5 kJ mol^{-1}) seems to be too small even if the tunneling is dominant, since it is smaller than the heat of reaction ($\Delta H^\circ_{0\mathrm{K}} = 83.1$ kJ mol^{-1}).

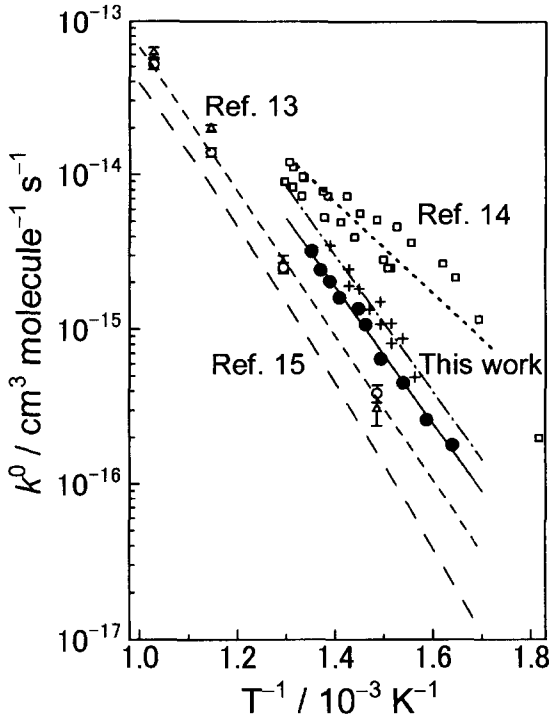

Fig. 5. Arrhenius plots of the second-order rate constants (k^0) for $CH_3O+M \rightarrow CH_2O+H+M$ (1a). Solid circles (●) and solid line (—): present results for M = He. Crossed (+) and dotted broken line (– · –): present results for M = N_2. Open circles (○) and open Triangles (△): Ref. 13 (M = Ar and N_2, respectively). Short dashed line (- - -): Ref. 13 (M = Ar, N_2, and Xe). Open squares (□) and dotted line (···): Ref. 14 (M = He). Long dashed line (— —): Ref. 15 (M = N_2).

The derived second-order rate constants for He and N_2 buffer, k^0(He) and $k^0(N_2)$, indicate the almost equal activation energies (84.3 and 84.1 kJ mol^{-1}, respectively) but larger pre-exponential factor for N_2. Since the collisional frequency is slightly smaller for N_2 buffer, this implies the larger efficiency of collisional energy transfer for N_2, which will be quantitatively analyzed in the next section.

Discussion

In order to confirm the validity of the present experimental results, as well as to understand the nature of the reaction, a quantitative comparison with the theoretical investigations and with the measurements of the state-resolved microcanonical rate constants by Dertinger et al.[22] is nec-

essary. Since a significant tunneling effect is expected for this hydrogen atom elimination reaction with a pronounced barrier, an RRKM calculation with proper treatment on the tunneling effect was performed.

A. RRKM Model with Tunneling Treatment: The molecular parameters used in the RRKM calculation are summarized in Table 1. Rotational constants and vibrational frequencies of methoxy (CH_3O) radical were taken from the spectroscopic studies.[28—30] Structures and vibrational frequencies of the transition states were estimated by DFT method, B3LYP/AUG-cc-pVTZ level, by using Gaussian98 program.[32] The frequencies were used without scaling since no scaling factor has been reported for B3LYP/AUG-cc-pVTZ level calculation, and since limited comparison with experimental frequencies for CH_2O and CH_2OH indicates no significant deviation from experiments, that is, the ratio of experimental to calculated frequencies was 0.995 ± 0.107 (error limit: 2 standard deviations).

The semiclassical tunneling correction[18,33,34] to the conventional RRKM expression for the microcanonical rate constant:

$$k_{CL}(E) = \frac{N(E-E_0)}{h\rho(E)} = \frac{\sum_n \varepsilon(E-E_n^{\ddagger})}{h\rho(E)} \quad (5)$$

involves replacing the step function, $\varepsilon(E-E_n^{\ddagger})$, with the quantum mechanical probability of transmission, $P(E-E_n^{\ddagger})$:

$$k_{QM}(E) = \frac{\sum_n P(E-E_n^{\ddagger})}{h\rho(E)}. \quad (6)$$

Here h is the Planck constant, E is the energy relative to the ground state of the reactant (CH_3O), E_0 is the threshold energy for the reaction, $E_n^{\ddagger}$ is the energy of the n'th vibrationally adiabatic channel of the transition state, $N(E-E_0)$ and $\rho(E)$ denote the sum of states of the transition state and the density of state of the reactant, respectively, at energy E. The transmission probability was evaluated by assuming a one-dimensional Eckart potential from the analytical expression.[35] The Eckart potential was constructed by giving three parameters: the energy difference between reactants and products, the threshold energy, and the second derivative at the top of the barrier (or imaginary frequency along the reaction coordinate). The reaction enthalpy at 0 K, ΔH_{0K}°, derived by the measurements of state-specific microcanonical rate constants,[22] which is good agreement with that derived by the photofragment translational energy spectroscopy,[36] was used in the calculation. The threshold energy for the C–H fission transition state was adjusted so as to fit the experimental results. Since the DFT calculation underestimates the barrier height for a backward reaction, $CH_2O+H \rightarrow CH_3O$, the calculated imaginary frequency, $578i$ cm^{-1}, was scaled to be $900i$ cm^{-1} by assuming the proportionality between the barrier height and the negative force constant. This scaling seems to be sound since the estimated imaginary frequency is in reasonable agreement with that estimated by Dertinger et al.,[22] $830i$ cm^{-1}, which was derived by the same scaling procedure, but from the frequency ($1435i$ cm^{-1}) calculated by MCSCF[19] which rather overestimates the barrier height. The estimated energy diagram for the reaction is shown in Fig. 6.

The collisional energy transfer was assumed to obey the exponential-down model.[37] The steady-state solution to the master equation was obtained by the conventional method by using *UNIMOL program suite*.[38] The average downward energy transferred per collision, $\langle\Delta E_{down}\rangle$, was adjusted so as to reproduce the experimental results.

B. RRKM Fit to the Experimental Results and the Tunneling Effect in the Low-pressure Limit: With the RRKM model described above, the threshold energy for the C–H bond fission process, E_0, and the average downward energy transferred per collision, $\langle\Delta E_{down}\rangle$, were derived by fitting to the experimental results shown in Fig. 4. The best fit was derived by a least-squares procedure, that is, by searching the minimum of the sum of square residuals on the two

Table 1. Molecular Parameters Used in the RRKM Calculation

Molecule	Vibrational frequencies / cm^{-1} a)	Rotational constants / cm^{-1}	Rotational symmetry number (Symmetry)	Degeneracy (Electronic state)
CH_3O	2840, 1362, 1047, 2774(2), 1487(2), 653(2)	5.176, 0.9329, 0.9329	3 (C_{3v})	4 (^2E)
TS($\rightarrow CH_2O + H$)[b]	2886, 1722, 1514, 1162, 351, 900i,[c] 2937, 1251, 403	3.376, 1.027, 0.9435	1 (C_s)	2 ($^2A'$)
TS($\rightarrow CH_2OH$)[b]	3042, 2410, 1475, 1144, 965, 2002i, 3151, 1135, 728	5.836, 0.9687, 0.9341	1 (C_s)	2 ($^2A'$)

L–J Parameters[d]	σ/Å	(ε/k_B)/K
CH_3O	3.63	481.8
He	2.55	10.22
N_2	3.798	71.4

a) Values in parentheses denote the degeneracy of the vibrational mode. b) Estimated by B3LYP/AUG-cc-pVTZ calculations without scaling except for the imaginary frequency for TS($\rightarrow CH_2O+H$). c) Scaled by assuming the proportionality between the barrier height and the force constant. d) L–J parameters for CH_3O were assumed to be the same as those of CH_3OH. All parameters have been taken from Ref. 31.

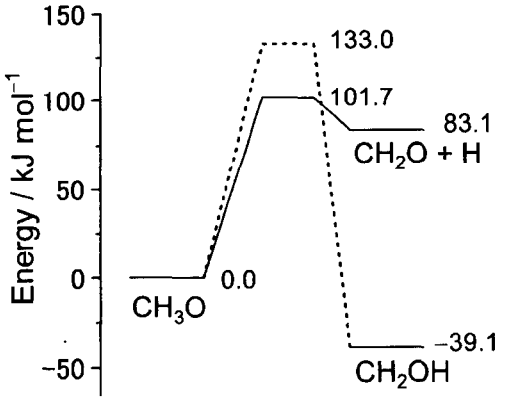

Fig. 6. Energy diagram for the unimolecular reactions of CH_3O.

dimensional surface. The best fit parameters were derived as: $E_0 = (101.7 \pm 1.3)$ kJ mol^{-1} and $\langle \Delta E_{down} \rangle = (210 \pm 22)$ cm^{-1}. The rate constants calculated with these parameters are shown in Fig. 7 by solid lines with experimental results. Experimental data for N_2 buffer gas were also analyzed with the same E_0 (= 101.7 kJ mol^{-1}) and $\langle \Delta E_{down} \rangle = (290 \pm 15)$ cm^{-1} was derived.

For comparison, an RRKM fit was also performed without tunneling treatment and is also shown in Fig. 7 by broken lines. The derived parameters without tunneling treatment were: $E_0 = 99.6$ kJ mol^{-1} and $\langle \Delta E_{down} \rangle = 358$ cm^{-1}. It should be noted that the calculated pressure dependence is apparently curved when the tunneling effect is included, while the classical RRKM calculation shows almost completely linear pressure dependence. This curvature in the pressure dependence can be explained as follows. As the pressure decreases, the effective threshold energy decreases, and thus the local derivative dk/dP (or local second-order rate constant) increases. This makes the pressure dependence curved. This situation is depicted in Fig. 8. The energy distribution of microcanonical reactive flux, $k(E)g(E)$ (where $k(E)$ and $g(E)$ denote the microcanonical rate constant and the steady-state population distribution, respectively), is plotted at several pressures. As the pressure decreases, the reactive flux shifts to lower energy region because the collisional excitation becomes inefficient, and, at the extremely low pressure, the effective threshold energy will match with the heat of reaction, ΔH°_{0K}. In other words, the *true* low-pressure limiting condition can only be achieved at extremely low pressures, and, when the tunneling effect is significant, the pressure dependence is rather in the fall-off region even under the classically complete low-pressure limiting conditions.

Although it is not so clear because of the scattering of the data, the experimental pressure dependence seems to be rather better reproduced by the RRKM calculation with tunneling treatment than by that without tunneling, since the positive intersections of the broken lines at $P = 0$ shown in Fig. 4 suggest the curved pressure dependence at lower pressure region, though the deviation from the straight line is not clearly seen in the experimental data obtained at pressures above 100 Torr. The second-order rate constants given in the previous section effectively express the pressure dependence of the rate constant in the measured pressure range (100—450 Torr), but it should be noted that, at least as the effective rate expression, the presence of the positive intersections at zero-pressures should be taken into account. Development

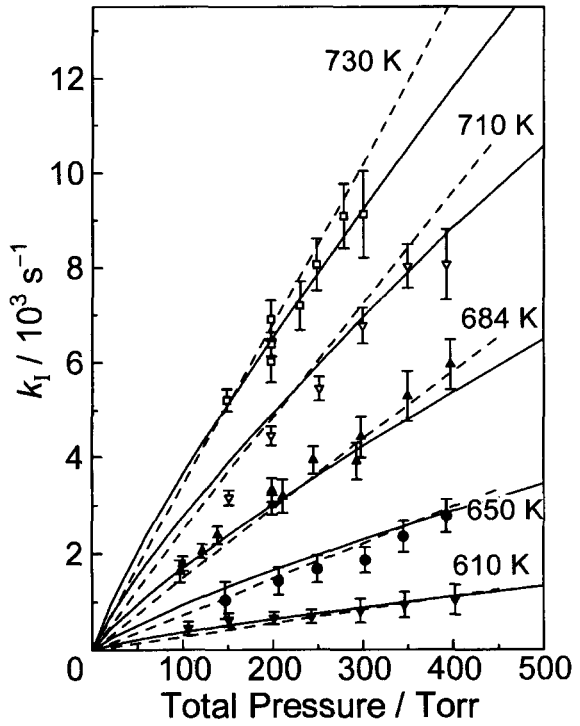

Fig. 7. Results of RRKM-fit with tunneling (—) and without tunneling (- - -). See text for detail.

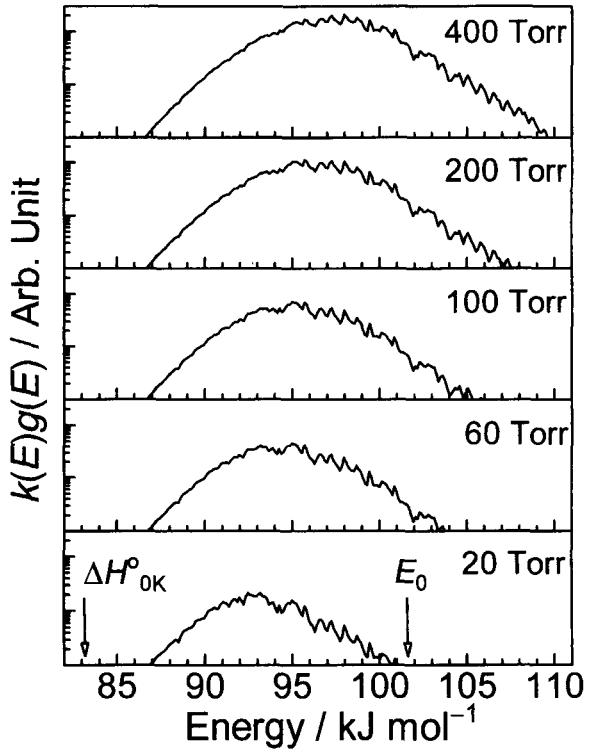

Fig. 8. Microcanonical reactive flux ($k(E)g(E)$) distributions (at 710 K, He buffer).

of more precise, physically meaningful rate expressions for such reaction processes will be needed.

The average downward energy transferred per collision derived here with tunneling treatment ($\langle\Delta E_{down}\rangle = 210$ cm^{-1}) seems reasonable in comparison with those derived for He buffer gas in the thermal decomposition of C_2H_5 (220—290 cm^{-1} at 880—1100 K),[39] n-C_3H_7 (220 cm^{-1} at 620—730 K),[40] i-C_3H_7 (210 cm^{-1} at 720—910 K),[41] and t-C_4H_9O (150 cm^{-1} at 303—393 K).[17] The temperature dependence of $\langle\Delta E_{down}\rangle$ was ignored in the present study since the measurements were done in narrow temperature range (610—740 K).

The RRKM model without tunneling may be useful as a crude approximation by setting the effectively lower threshold energy. However, the fit to the experimental data resulted in the too high estimate of $\langle\Delta E_{down}\rangle$ (= 358 cm^{-1}) because it could not represent the broad energy dependence of $k(E)$ around the threshold energy (see below). Further, of course, it could not reproduce the curved pressure dependence at low-pressure region.

C. Comparison with Theoretical Studies and with State-Specific Rate Constants Measured by SEP: Enthalpy of the reaction at 0 K, ΔH°_{0K}, used in the present calculation, and the threshold energy, E_0, derived in the present study are compared with theoretical values in Table 2. The G2 and B3LYP/AUG-cc-pVTZ calculations were done in the present study by using Gaussian94 or Gaussian98.[32] All of the theoretical results with high electron correlation method (MRCI, CCI+Q, and G2) predict smaller ΔH°_{0K} than the experimental one. Major part of these errors seems to come from the inaccuracy of the zero-point energy (ZPE) of CH_3O based on the SCF level frequency calculations. It should be noted that even the B3LYP model, which in general predicts the vibrational frequencies with high accuracy,[42] overestimates the ZPE, maybe because the local force constants are calculated at $^2A'$ minimum while, from the spectroscopy, the electronic state is ^2E in C_{3v} symmetry, with the Jahn–Teller splitting smaller than the zero-point vibration.[43] By replacing the ZPE's with experimental ones (values shown in brackets in Table 2), better agreement was found with experimental ΔH°_{0K}. For the same reason, E_0 values corrected with experimental ZPE of CH_3O and B3LYP/AUG-cc-pVTZ ZPE of the transition state are shown in brackets. The ZPE-corrected threshold energies by G2 (100.5 kJ mol^{-1}) and CCI+Q (102.4 kJ mol^{-1}) agree quite well with the value derived in the present study. Also the threshold energy derived from the state-specific rate constant measurements[22] (101.68 kJ mol^{-1}) agrees well with the present value.

In Fig. 9, the microcanonical rate constants, $k(E)$, calculated from the present RRKM model are compared with the averaged state-specific rate constants measured by the SEP method.[22] The present RRKM model well agrees with these direct measurement of $k(E)$. In other words, the present experimental results are consistent with the directly measured $k(E)$.

These consistencies support the validity of the present measurements and estimated magnitude of the tunneling effect in the present RRKM model.

D. Estimate of the Contribution of the Isomerization

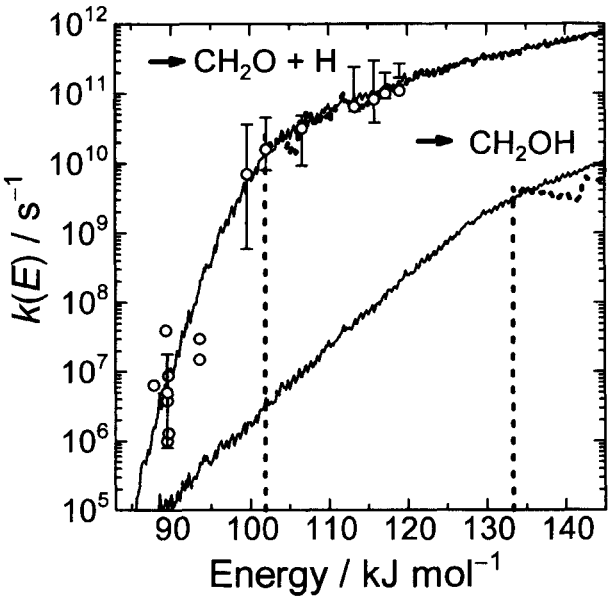

Fig. 9. Microcanonical rate constants ($k(E)$) for channels (1a) ($\rightarrow CH_2O+H$) and (1b) ($\rightarrow CH_2OH$). Dotted lines denote those calculated without tunneling. Open circles (○) denote the microcanonical rate constants reported in Ref. 22.

Table 2. Heat of Reaction and Threshold Energy for the Unimolecular Reaction of $CH_3O \rightarrow CH_2O+H$[a)]

Method	ΔH°_{0K}	E_0	ZPE(CH_3O)[b)]	ZPE(CH_2O)[b)]	ZPE(TS)[b)]	Reference
MRCI/TZP	73.6	107.1	102.9	74.5	81.2	18
//MCSCF/DZP	[79.3][c)]	[111.5][c)]				
CCI+Q/cc-pVTZ	74.5	97.9	102.5	73.7	80.7	19
//CASSCF/cc-pVDZ	[80.6][c)]	[102.4][c)]				
G2	75.1	95.4	94.4	68.5	72.0	20, This work
	[78.3][c)]	[100.5][c)]				
B3LYP	102.0	111.6	94.7	69.6	73.1	This work
/AUG-cc-pVTZ						
Experimental	(83.1 ± 5.3)[d)]	101.7 ± 1.3	(90.4)[e)]	(67.7)[e)]	(73.1)[f)]	This work

a) In the unit of kJ mol^{-1}. b) Zelo-point vibrational energies. c) Values in bracket denote the corrected values by using experimetnal (or DFT) frequencies for the zero-point energy. See text for detail. d) From Ref. 22. e) Calculated from experimental frequencies.[29,30] f) Unscaled B3LYP/AUG-cc-pVTZ frequencies were used as the best estimate.

Channel (1b): Although the threshold energy for the isomerization channel (1b) is predicted to be higher than the C–H fission channel (1a), a larger tunneling effect is expected for the exothermic isomerization channel (1b). Thus the contribution of this channel was assessed by an RRKM calculation based on the theoretical results. Properties of the transition state were also listed in Table 1. The structure and the vibrational frequencies were estimated at B3LYP/AUG-cc-pVTZ level calculation. Since the calculation at this level predicts the potential energy barrier (140.6 kJ mol^{-1}) in good agreement with higher level calculations (139.4 kJ mol^{-1} at CCI+Q/cc-pVTZ//CASSCF/cc-pVDZ level[19] and 138.2 kJ mol^{-1} at G2 level[20]), the calculated imaginary frequency was used without scaling to construct the Eckart potential. The heat of the reaction was estimated to be $\Delta H^{\circ}_{0K}(1b) = -39.1$ kJ mol^{-1} based on the experimental heats of formation. The threshold energy was estimated to be $E_0(1b) = 133.0$ kJ mol^{-1}, which is CCI+Q/cc-pVTZ//CASSCF/cc-pVDZ level calculation[19] corrected with experimental ZPE of CH_3O and B3LYP/AUG-cc-pVTZ ZPE of the transition state. The calculated microcanonical rate constant, as shown in Fig. 9, is more than one order of magnitude smaller than that for C–H fission channel (1a) except at the very low energy region below ca. 85 kJ mol^{-1}. A multichannel RRKM calculation estimates that the branching fraction for 1b is small ($<1.4\%$) in the present experimental conditions. The contribution of the isomerization process will be negligible except at very low pressures.

Conclusion

1) The thermal unimolecular decomposition of the methoxy radicals (1a) has been directly investigated by laser induced fluorescence method. The measured second order rate constants were significantly lower than those reported by Choudhury et al.[14]

2) The RRKM calculation with tunneling treatment indicates the characteristic nonlinear pressure dependence of the rate constants at the classical low-pressure limit, which is consistent with the experimental results. Development of the rate expressions for this type of reaction will be needed.

3) Analysis with an RRKM calculation showed that the present results are in good agreement with the theoretical calculations and with the direct measurements of the microcanonical rate constants, and that the tunneling effect is very important in this reaction.

4) The contribution of the isomerization process (1b) was estimated to be minor by the RRKM calculation based on the theoretical investigations.

References

1 G. Inoue, H. Akimoto, and M. Okuda, *J. Chem. Phys.*, **72**, 1769 (1980).

2 D. Gutman, N. Sanders, and J. E. Butler, *J. Phys. Chem.*, **86**, 66 (1982).

3 K. Lorenz, D. Rhäsa, R. Zellner, and B. Fritz, *Ber. Bunsenges. Phys. Chem.*, **89**, 341 (1985).

4 P. J. Wantuck, R. C. Oldenborg, S. L. Baughcum, and K. R. Winn, *J. Phys. Chem.*, **91**, 4653 (1987).

5 J. A. McCaulley, S. M. Anderson, J. B. Jeffries, and F. Kaufman, *Chem. Phys. Lett.*, **115**, 180 (1985).

6 M. J. Frost and I. W. M. Smith, *J. Chem. Soc., Faraday Trans.*, **86**, 1751 (1990).

7 P. Biggs, C. E. Canosa-Mas, J.-M. Fracheboud, A. D. Parr, D. E. Shallcross, R. P. Wayne, and F. Caralp, *J. Chem. Soc., Faraday Trans.*, **89**, 4163 (1993).

8 N. Sanders, J. E. Butler, L. R. Pasternack, and J. R. McDonald, *Chem. Phys. Lett.*, **49**, 17 (1980).

9 P. Morabito and J. Heicklen, *J. Phys. Chem.*, **89**, 2914 (1985).

10 M. J. Frost and I. W. M. Smith, *J. Chem. Soc., Faraday Trans.*, **86**, 1757 (1990).

11 J. A. McCaulley, A. M. Moyle, M. F. Golde, S. M. Anderson, and F. Kaufman, *J. Chem. Soc., Faraday Trans.*, **86**, 4001 (1990).

12 K. Ohmori, K. Yamsaki, and H. Matsui, *Bull. Chem. Soc. Jpn.*, **66**, 51 (1993).

13 P. J. Wantuck, R. C. Oldenborg, S. L. Baughcum, and K. R. Winn, *Proc. Symp. (Int.) Combust.*, **22**, 973 (1988).

14 T. K. Choudhury, Y. He, W. A. Sanders, and M. C. Lin, *J. Phys. Chem.*, **94**, 2394 (1990).

15 W. Tsang and R. F. Hampson, *J. Phys. Chem. Ref. Data*, **15**, 1087 (1986).

16 P. Devolder, Ch. Fittschen, A. Frenzel, H. Hippler, G. Poskrebyshev, F. Striebel, and B. Visjolcz, *Phys. Chem. Chem. Phys.*, **1**, 675 (1999).

17 M. Blitz, M. J. Pilling, S. H. Robertson, and P. W. Seakins, *Phys. Chem. Chem. Phys.*, **1**, 73 (1999).

18 M. Page, M. C. Lin, Y. He, and T. K. Choudhury, *J. Phys. Chem.*, **93**, 4404 (1989).

19 S. Walch, *J. Chem. Phys.*, **98**, 3076 (1993).

20 L. A. Curtiss, L. D. Kock, and J. A. Pople, *J. Chem. Phys.*, **95**, 4040 (1991).

21 a) A. Geers, J. Kappert, F. Temps, and J. W. Wiebrecht, *J. Chem. Phys.*, **101**, 3618 (1994). b) A. Geers, J. Kappert, F. Temps, and J. W. Wiebrecht, *J. Chem. Phys.*, **101**, 3634 (1994).

22 S. Dertinger, A. Geers, J. Kappert, J. Wiebrecht, and F. Temps, *Faraday Discuss.*, **102**, 31 (1995).

23 M. Koshi, N. Nishida, Y. Murakami, and H. Matsui, *J. Phys. Chem.*, **97**, 4473 (1993).

24 S. Satyapal, J. Park, R. Berson, and B. Katz, *J. Chem. Phys.*, **91**, 6873 (1989).

25 S. Okada, A. Tezaki, K. Yamasaki, and H. Matsui, *J. Chem. Phys.*, **98**, 8667 (1993).

26 D. L. Baulch, C. J. Cobos, R. A. Cox, P. Frank, G. Hayman, Th. Just, J. A. Kerr, T. Murrells, M. J. Pilling, J. Troe, R. W. Walker, and J. Warnatz, *J. Phys. Chem. Ref. Data*, **23**, 847 (1994).

27 G. Lendvay, T. Bérces, and F. Márta, *J. Phys. Chem. A*, **101**, 1588 (1997).

28 Y. Endo, S. Saito, and E. Hirota, *J. Chem. Phys.*, **81**, 122 (1984).

29 S. C. Foster, P. Misra, T.-Y. D. Lin, C. P. Damo, C. C. Carter, and T. A. Miller, *J. Phys. Chem.*, **92**, 5914 (1988).

30 Y.-Y. Lee, G.-H. Wann, and Y.-P. Lee, *J. Chem. Phys.*, **99**, 9465 (1993).

31 E. L. Cussler, "DIFFUSION," Cambridge University Press, New York (1984), p. 110.

32 "Gaussian98 (Rev. A.5)," M. J. Frisch, G. W. Trucks, H. B. Schlegel, G. E. Scuseria, M. A. Robb, J. R. Cheeseman, V. G. Zakrzewski, J. A. Montgomery, R. E. Stratmann, J. C. Burant, S.

Dapprich, J. M. Millam, A. D. Daniels, K. N. Kudin, M. C. Strain, O. Farkas, J. Tomasi, V. Barone, M. Cossi, R. Cammi, B. Mennucci, C. Pomelli, C. Adamo, S. Clifford, J. Ochterski, G. A. Petersson, P. Y. Ayala, Q. Cui, K. Morokuma, D. K. Malick, A. D. Rabuck, K. Raghavachari, J. B. Foresman, J. Cioslowski, J. V. Ortiz, B. B. Stefanov, G. Liu, A. Liashenko, P. Piskorz, I. Komaromi, R. Gomperts, R. L. Martin, D. J. Fox, T. Keith, M. A. Al-Laham, C. Y. Peng, A. Nanayakkara, C. Gonzalez, M. Challacombe, P. M. W. Gill, B. G. Johnson, W. Chen, M. W. Wong, J. L. Andres, M. Head-Gordon, E. S. Replogle, and J. A. Pople, Gaussian, Inc., Pittsburgh, PA (1998).

33 B. C. Garrett and D. G. Truhlar, *J. Phys. Chem.*, **83**, 2921 (1979).

34 W. H. Miller, *J. Am. Chem. Soc.*, **101**, 6810 (1979).

35 a) C. Eckart, *Phys. Rev.*, **35**, 1303 (1930). b) H. Johnston and J. Heicklen, *J. Phys. Chem.*, **66**, 532 (1962).

36 D. L. Osborn, D. J. Leahy, E. M. Ross, and D. M. Neumark, *Chem. Phys. Lett.*, **235**, 484 (1995).

37 R. G. Gilbert and S. C. Smith, "Theory of Unimolecular and Recombination Reactions," Blackwell, Oxford (1990).

38 R. G. Gilbert, S. C. Smith, and M. J. T. Jordan, "UNIMOL Program Suite (Calculation of Fall-Off Curves for Unimolecular and Recombination Reactions)," (1993). Available from the authors: School of Chemistry, Sydney University, NSW 2006, Australia or by e-mail to: gilbert_r@summer.chem.su.oz.au.

39 Y. Feng, J. T. Niiranen, Á. Bencsura, V. D. Knyazev, and D. Gutman, *J. Phys. Chem.*, **97**, 871 (1993).

40 Á Bencsura, V. D. Knyazev, S.-B. Xing, I. R. Slagle, and D. Gutman, *Proc. Symp. (Int.) Combust.*, **24**, 629 (1992).

41 P. W. Seakins, S. H. Robertson, M. J. Pilling, I. R. Slagle, G. W. Gmurczek, Á Bencsura, D. Gutman, and W. Tsang, *J. Phys. Chem.*, **97**, 4450 (1993).

42 P. J. Stevens, F. J. Devlin, C. F. Chablowski, and M. J. Frisch, *J. Phys. Chem.*, **98**, 11623 (1994).

43 S. Saebø, L. Radom, and H. F. Schaefer, III, *J. Chem. Phys.*, **78**, 845 (1983).